

# Recent decline in extratropical lower stratospheric ozone attributed to circulation changes

Krzysztof Wargan<sup>1,2</sup>, Clara Orbe<sup>3</sup>, Steven Pawson<sup>2</sup>, Jerald R. Ziemke<sup>4,5</sup>, Luke D. Oman<sup>3</sup>, Mark A. Olsen<sup>4,5</sup>, Lawrence Coy<sup>1,2</sup>, K. Emma Knowland<sup>6,2</sup>

<sup>1</sup> Science Systems and Applications Inc., Lanham, Maryland, USA

<sup>2</sup> Global Modeling and Assimilation Office, Code 610.1, NASA Goddard Space Flight Center, Greenbelt, Maryland, USA

<sup>3</sup> Code 611, NASA Goddard Institute for Space Studies, New York, NY, USA

<sup>4</sup> Goddard Earth Science Technology & Research (GESTAR) Morgan State University, Baltimore, MD USA

<sup>5</sup> Atmospheric Chemistry and Dynamics Laboratory, Code 614, NASA Goddard Space Flight Center, Greenbelt, Maryland, USA

<sup>6</sup> Goddard Earth Science Technology & Research (GESTAR), Universities Space Research Association (USRA), Columbia, MD USA

Corresponding author: Krzysztof Wargan ([Krzysztof.Wargan-1@nasa.gov](mailto:Krzysztof.Wargan-1@nasa.gov))

## Key Points:

- The MERRA-2 reanalysis shows negative ozone trends in the extratropical lower stratosphere between 1998 and 2016.
- These ozone trends are likely a result of enhanced two-way transport between the Tropics and the extratropics.
- This study is the first to use bias-corrected reanalysis ozone to assess and attribute vertically-resolved ozone trends.

## Abstract

1998-2016 ozone trends in the lower stratosphere (LS) are examined using the Modern-Era Retrospective Analysis for Research and Applications Version 2 (MERRA-2) and related NASA products. After removing biases resulting from step-changes in the MERRA-2 ozone observations, a discernible negative trend of  $-1.67 \pm 0.54$  Dobson units per decade (DU/decade) is found in the 10-km layer above the tropopause between  $20^\circ\text{N}$  and  $60^\circ\text{N}$ . A weaker but statistically significant trend of  $-1.17 \pm 0.33$  DU/decade exists between  $50^\circ\text{S}$  and  $20^\circ\text{S}$ . In the Tropics, a positive trend is seen in a 5-km layer above the tropopause. Analysis of an idealized tracer in a model simulation constrained by MERRA-2 meteorological fields provides strong evidence that these trends are driven by enhanced isentropic transport between the tropical ( $20^\circ\text{S}$ – $20^\circ\text{N}$ ) and extratropical LS in the past two decades. This is the first time that a reanalysis dataset has been used to detect and attribute trends in lower stratospheric ozone.

## Plain Language Summary

Stratospheric ozone shields the biosphere from harmful ultraviolet radiation and affects the Earth's radiative budget. Observational data show evidence that concentrations of ozone in the upper stratosphere have increased in the last 15 years. This is an expected result of the implementation of the Montreal Protocol and its amendments banning emissions of ozone depleting substances into the atmosphere. The evolution of stratospheric ozone is also impacted by climate change through its dependence on temperature and circulation, which can be different at different altitudes. These effects are less well understood. This study uses NASA's data and computer models to analyze the long-term changes in ozone since 1998. It is shown that the increase in the upper-stratospheric ozone has been partially offset by a small but discernible decline of ozone concentrations in the lowermost stratosphere, in qualitative agreement with one recent study. A chemistry model simulation forced by meteorological data provides strong evidence that the primary mechanism driving this negative trend is an intensification of transport of ozone-poor air from the tropics into the extratropics, indicative of a systematic change in the lower-stratospheric circulation between 1998 and 2016.

## 1. Introduction

The projected decadal-scale evolution of stratospheric ozone in the 21<sup>st</sup> century results from an interplay between human-induced changes in both atmospheric composition and the circulation (WMO, 2014). There is already observational evidence of a positive trend (between about 2000 and 2015) in upper stratospheric ozone. While this is consistent with model projections (Eyring et al., 2010; Oman et al., 2010), and attributed to both decreases in ozone depleting substance (ODS) concentrations and cooling caused by increased greenhouse gases, the estimated trends vary in magnitude and statistical significance (Bourassa et al., 2014, WMO 2014, Harris et al., 2015, Ball et al., 2017, Sofieva et al., 2017, Steinbrecht et al., 2017). No significant signal of ozone recovery was found in the lower stratosphere (LS) (WMO 2014). Despite the ODS decreases since 1998, Randel and Thompson (2011) found a negative trend in ozonesonde and satellite ozone data in the tropical LS between 1984 and 2005, which they attributed to increases in upwelling. Using merged and drift-corrected satellite data, Bourassa et al (2014; 2018) reported negative trends in post-1997 ozone at and below 20 km between 40°S and 40°N. Sofieva et al. (2017) and Steinbrecht et al. (2017) also found evidence for declining ozone in the lowermost stratosphere, although there are large uncertainties in these trends. Ball et al. (2018) identified a statistically significant decline of LS ozone between 60°S and 60°N between 1998 and 2016. Using dynamical linear regression, they found a negative change of approximately 2 Dobson units (DU) in ozone partial column between the tropopause and 24 km. This decrease more than offsets the positive trend in the upper stratosphere, leading to a continuing decline of the stratospheric ozone column.

The present study isolates the LS ozone trends in the Modern-Era Retrospective analysis for Research and Applications, Version 2 (MERRA-2: Gelaro et al., 2017) and related assimilated products. Additionally, a chemical model simulation driven by MERRA-2 is used to link these trends to decadal-scale changes in stratospheric transport. As MERRA-2 assimilates data from Solar Backscatter Ultraviolet (SBUV) radiometers and the Microwave Limb Sounder (MLS: Waters et al., 2006; Froidevaux et al., 2008), it is not entirely independent from other (cited) trend analyses, which also utilize merged satellite data including SBUV and MLS. However, the application of data assimilation methodology allows a relatively high vertical resolution of the reanalysis product and facilitates interpretation of the ozone behavior in terms of variability and trends in the atmospheric circulation, provided that biases resulting from step-changes in its observing system are removed. While some recent studies assessed trends in total column ozone in reanalyses (Bai et al., 2017, de Laat et al., 2017) the use of a bias-corrected reanalysis to derive vertically resolved ozone trends in the LS in the context of transport patterns is a novel part of this work.

This analysis spans the latitudes between 60°S and 60°N broadly divided into the Tropics (20°S–20°N) and the extratropics (60°S–20°S and 20°N–60°N). The LS is defined as the 10-km layer immediately above the tropopause, which corresponds to an upper boundary of approximately 50 hPa in the extratropics. In light of the results presented below, this definition allows a clear separation between different ozone trend regimes, although it differs from that of Ball et al. (2018) who consider the layer between 147 hPa and 32 hPa in the extratropics and between 100 hPa and 32 hPa in the Tropics.

Section 2 describes the data and methodology. The trend calculations are presented in Section 3. Section 4 is devoted to an analysis of tracer transport in the LS. A discussion of the findings is presented with the conclusions in Section 5.

## **2. Data and Methods**

### **2.1. The GEOS Products**

MERRA-2 (Gelaro et al., 2017; Bosilovich et al., 2015) is a global atmospheric reanalysis spanning the period from 1980 to (presently) 2018. It uses the Goddard Earth Observing System (GEOS) Version 5 general circulation model (e.g., Molod et al., 2015) and the Gridpoint Statistical Interpolation (GSI) scheme that performs three-dimensional variational assimilation of observations (Wu et al., 2002; Kleist et al., 2009). The reanalysis is done on a  $0.5^\circ \times 0.625^\circ$  latitude/longitude grid on 72 layers between the surface and 0.01 hPa. The vertical resolution in the upper troposphere (UT) and LS is about 1.1 km.

The MERRA-2 ozone products are described and evaluated in Wargan et al. (2017), McCarty et al. (2016) and Davis et al. (2017). MERRA-2 assimilates partial column ozone from a series of SBUV instruments between 1980 and September 2004. After September 2004, SBUV data are replaced by total ozone observations from the Ozone Monitoring Instrument (OMI: Levelt et al., 2006) and stratospheric ozone profiles from MLS onboard NASA's Aura satellite. This abrupt change from SBUV to Aura data needs to be taken into account when deriving long-term ozone changes from MERRA-2. Other discontinuities are a change from version 2.2 to 4.2 of MLS data in June 2015, the turning off of the lowest assimilated MLS level (261 hPa) in May 2016 and step-changes in the assimilated radiance data. Wargan et al. (2017) found a very good agreement between MERRA-2 ozone and ozonesonde observations in the UT and LS; in particular, there is an accurate representation of the cross-tropopause ozone gradients and variability on daily-to-interannual time scales. This study uses three-hourly MERRA-2 ozone, temperature, height and potential vorticity output on native model levels (GMAO, 2015a) and monthly averaged ozone fields on pressure levels (GMAO, 2015b).

The GEOS-RPIT (Reprocessing for Instrument Teams) is a GMAO product that is generated using the MERRA-2 system, but which does not assimilate MLS ozone observations. GEOS-RPIT uses OMI total column ozone from October 2004 but assimilates the Version 8.6 SBUV ozone until December 2010 and switches to the older version 8.0 afterwards. Other differences from MERRA-2, including the sea surface temperature boundary conditions, have negligible impact on the ozone fields. The absence of high-vertical-resolution MLS data reduces the discontinuity arising from the introduction of Aura data in MERRA-2. Therefore, using GEOS-RPIT and MERRA-2 together increases the confidence in any results that pertain to long-term LS ozone changes. Since GEOS-RPIT and MERRA-2 ozone fields are almost the same before 1 October 2004 this study fills in the period before that date with the MERRA-2 ozone analyses (hereafter, this MERRA-2–GEOS-RPIT blend is referred to simply as GEOS-RPIT).

The MERRA-2 Global Modeling Initiative (M2-GMI) is a GEOS simulation that is constrained with MERRA-2 meteorological fields (but not by MERRA-2 ozone) and uses the GMI chemical mechanism (Douglass et al., 2004; Nielsen et al., 2017). It uses the “replay” methodology, where increments are calculated from the assimilated horizontal winds, temperature and pressure and

applied as a forcing to the meteorology at every model time step (Bloom et al., 1996, Orbe et al., 2017). As demonstrated by Orbe et al. (2017), this method of constraining the model’s large-scale flow produces realistic stratospheric mean ages and vertical transport properties in the Tropics. Several idealized tracers were also included in the simulation, including an “e90” tracer (Prather et al., 2011) that is emitted globally at the surface and decays exponentially at a rate of 90<sup>-1</sup> days<sup>-1</sup> throughout the entire atmosphere.

Hereafter, the MERRA-2, M2-GMI and GEOS-RPIT datasets are referred to collectively as the “GEOS products”.

## 2.2. Ozonesondes

Data from electrochemical concentration cell ozonesondes are used from three locations: Trinidad Head, California (124.2°W, 41.1°N), Boulder, Colorado (105.2°W, 40°N) and Pago Pago, American Samoa (170.7°W, 14.3°S). This limited selection is motivated by the need to use data records suitable for trend analyses and located in the regions of interest. Ozonesonde data do not always meet that criterion owing to changes in sensing solutions and sonde types (Hubert et al., 2016; Thompson et al., 2017; Witte et al., 2017). The data used here (Sterling et al., 2017) were recently reprocessed with the “SkySonde” algorithm to correct for these changes. In particular, these homogenized ozonesonde records are suitable for studies of ozone changes on multidecadal time scales. One-sigma average uncertainty for these data is estimated at ±4–6% in the stratosphere and ±5–20% in the troposphere for individual soundings (Sterling et al., 2017).

## 2.3. Vertical Coordinates

Ozone trends have been computed in both absolute pressure and tropopause-relative (TR) coordinates. Pressure-level calculations were done on eight levels between 350 and 50 hPa for MERRA-2 and GEOS-RPIT and 10 levels for M2-GMI. For the TR coordinates, fields were remapped from the native GEOS grid as follows. At each grid point, the tropopause was calculated from the MERRA-2 meteorological fields on the native model layers. The tropopause was defined as the 2-potential vorticity unit (1 PVU = 10<sup>-6</sup> K kg<sup>-1</sup> m<sup>2</sup> s<sup>-1</sup>) isopleth or the 380-K potential temperature surface, whichever had the lower altitude. Ozone and e90 profiles were then interpolated from the model grid to the TR coordinate with 1 km vertical spacing, prior to zonal averaging.

## 2.4. Multiple linear regression

Trends were derived using the multiple linear regression (MLR) model from Stolarski et al. (1991):

(1)

$$y(t) = \alpha_0(t) + \alpha_1(t)t + \alpha_2(t)QBO_1(t) + \alpha_3(t)QBO_2(t) + \alpha_4(t)RF_{10.7}(t) + \alpha_5(t)MEI(t) + \alpha_6(t)AERO(t) + \epsilon(t)$$

where  $y(t)$  denotes the variable of interest,  $t$  stands for time in months and each of the coefficients,  $\alpha = \alpha_0, \alpha_1, \dots, \alpha_6$ , is the sum of a constant and the first two seasonal harmonics:

$$\alpha(t) = c + \sum_{k=1}^2 a_k \cos \frac{2k\pi t}{12} + b_k \sin \frac{2k\pi t}{12}$$

The proxies are the first two principal components of the Quasi-Biennial Oscillation (QBO, and QBO: Wallace et al., 1993) computed using winds from the Singapore radiosonde data (Naujokat, 1986), the 10.7 cm solar radio flux ( $RF_{10.7}$ : National Research Council Canada), latitude-resolved aerosol optical depth at 550 nm (AERO: Thomason et al., 2018) and Multivariate ENSO Index (MEI: Wolter and Timlin, 1998). A sensitivity test with Mg doublet index (280 nm) from the University of Bremen replacing  $RF_{10.7}$  yielded almost exactly the same MERRA-2 ozone trends. The residual is denoted by  $\epsilon(t)$ . The coefficient  $\alpha_1$  takes 12 values representing trends for each month of the year. In most cases, annually averaged trends are discussed. Statistical significance was assessed at the 2-sigma level assuming a first-order, auto-regressive model for the residuals (Weatherhead et al., 1998).

Cross-correlations between the proxies used in Equation (1) and a linear trend are less than 0.3 except for the  $RF_{10.7}$  (correlation of -0.4) and AERO, which exhibits a latitude-dependent correlation from 0.4 in the northern extratropics to 0.75 south of 55°S.

## 2.5. Bias correction

Step changes in MERRA-2 and GEOS-RPIT ozone were corrected by using a transfer function approach similar to Hegglin et al. (2014). This methodology exploits the absence of major discontinuities in M2-GMI allowing it to serve as a common baseline, against which discontinuities in the assimilated datasets were computed and removed. These corrections were applied to the step changes in the ozone observing systems in MERRA-2 and GEOS-RPIT delineated in Section 2.1. The period between June 2015 and April 2016, when MERRA-2 assimilated MLS ozone at the 261 hPa level, was excluded from the MERRA-2 ozone trend calculations. Details of the bias correction procedure are provided in the supporting information.

Changes in the meteorological observing system used in MERRA-2 can also have an effect on ozone, including in M2-GMI. Long et al. (2017) demonstrated that reanalysis stratospheric temperatures were most affected by the introduction of the Advanced Microwave Sounding Unit radiances in 1998. This study exclusively focuses on the period 1998-2016 to minimize that effect. Additional discussion of the potential impact of the observing system changes is presented in Section 5.

### 3. Results: Ozone trends in the LS

Figure 1 shows the time series of annually averaged ozone anomalies from ozonesondes, MERRA-2, GEOS-RPIT and M2-GMI at three ozonesonde locations at 70 hPa, 100 hPa, and 200 hPa, except for the tropical location, Pago Pago for which the 200-hPa result is not shown as it lies deeply in the troposphere, where the reanalysis quality is degraded (Wargan et al. 2017). All three GEOS products capture the interannual variability seen in the sonde data, with MERRA-2 and M2GMI agreeing better with the sondes than GEOS-RPIT (Figure 1); the coefficient of determination,  $r^2$ , ranges for MERRA-2 from 0.42 to 0.95, for M2GMI from 0.62 to 0.93, and for GEOS-RPIT from 0.14 to 0.85. The least-squares linear fit to the data has a negative slope at all three levels for Trinidad Head and Boulder, with GEOS-RPIT producing steeper slopes than MERRA-2 and the ozonesondes at the two upper levels. At the tropical site Pago Pago the ozonesonde and MERRA-2 and M2GMI at 70 hPa slopes are positive. We emphasize the different signs of the slopes between the tropical (positive) and extratropical (negative) locations at 70 hPa (Figure 1a-c). At 100 hPa all the slopes are close to zero but the agreement between the GEOS products and the ozonesondes is very good. Except for Boulder at 100 hPa, the slopes calculated from the sonde data are not significantly different from zero at the 2-sigma level. As a result of bias correction, no discernible jumps are seen in MERRA-2 or GEOS-RPIT compared to the sondes. Together with the findings of Wargan et al. (2017) these results provide confidence in the representation of LS ozone in MERRA-2 and, to some extent, in the other two GEOS products.

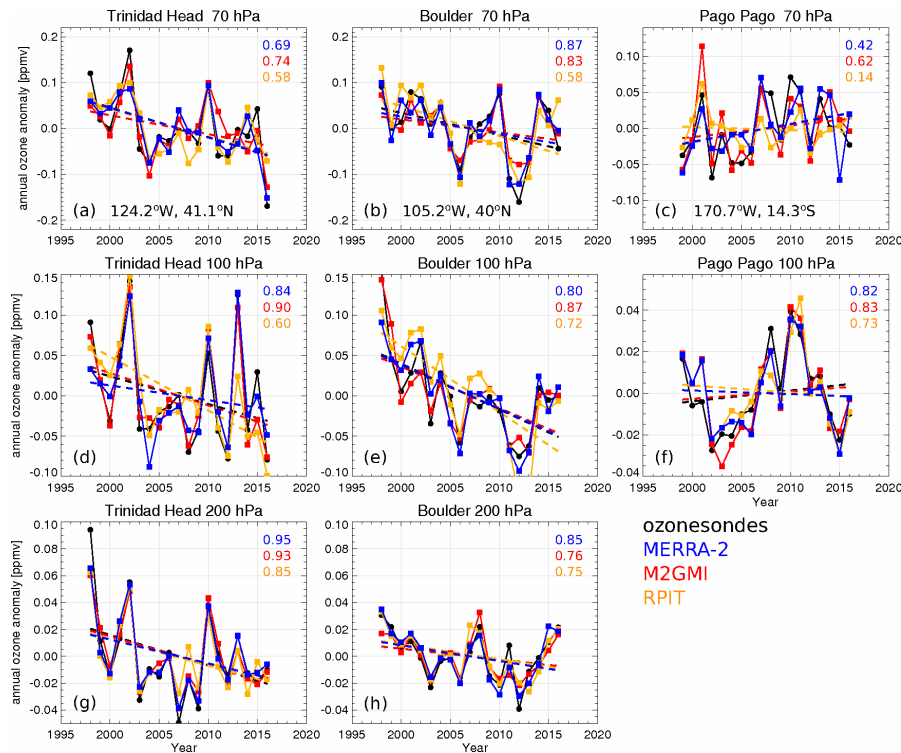
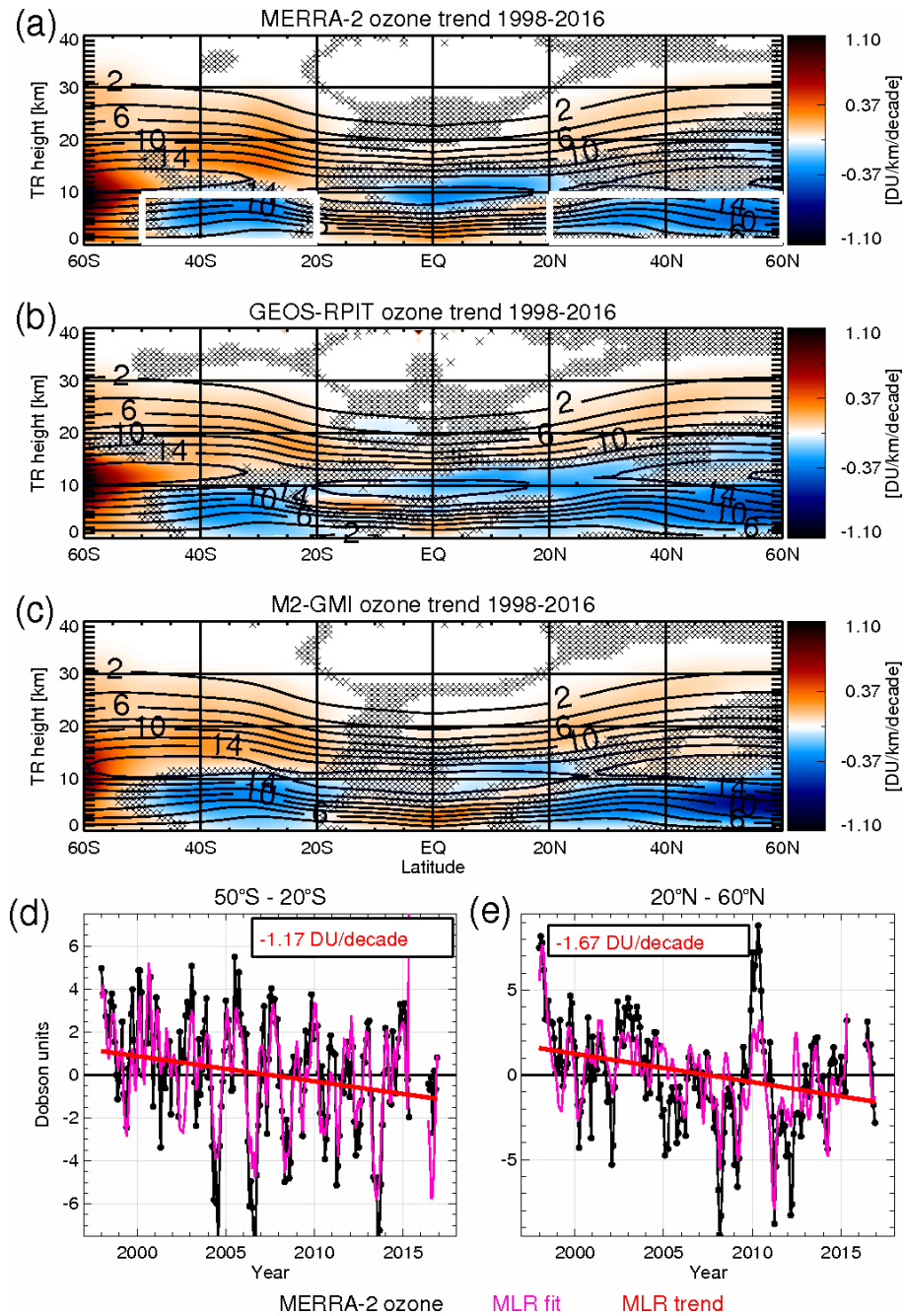


**Figure 1.** Time series of annual ozone anomalies at Trinidad Head (a, d, g), Boulder (b, e, h) and Pago Pago (c, f) at 70 hPa (a, b, c), 100 hPa (d, e, f) and 200 hPa (g, h) from ozonesondes (black), bias-corrected MERRA-2 (blue), M2-GMI (red) and bias-corrected GEOS-RPIT (yellow). The anomalies for each data set are calculated by subtracting the average of that data set. The corresponding least-squares fit lines are dashed and the  $R^2$  values are shown in each panel.



266

267

268

269

270

271

272

273

274

275

276

**Figure 2. (a-c):** Zonally and annually averaged ozone trends as a function of latitude and height above the tropopause derived from (a) MERRA-2, (b) GEOS-RPIT and (c) M2-GMI using multiple linear regression (colors). Averaged ozone in DU km<sup>-1</sup> is shown as contours. Locations where the trend is not significant at the 2-sigma level are marked by 'X'. (d-e): Time series of deseasonalized partial column ozone from MERRA-2 between 0.5 km and 9.5 km above the tropopause (black) averaged between (d) 50°S – 20°S and (e) 20°N – 60°N (within the white boxes in panel a). The magenta curves show ozone reconstructed from the MLR coefficients and the trends averaged over the same latitude bands are shown in red.



Annually averaged MLR trends between 60°S and 60°N are shown in DU decade<sup>-1</sup> in TR coordinates in Figure 2. MERRA-2, GEOS-RPIT and M2-GMI show similar patterns of ozone trends in the stratosphere. The positive trend in the middle stratosphere is consistent with the decreasing stratospheric ODS loading (WMO, 2014). Regions of statistically significant negative trends are evident in the extratropics in the LS in the southern and northern hemispheres (SH and NH, respectively). In the Tropics, the GEOS products show a positive trend in the 0–5 km TR layer below and a negative trend in the 5–10 km layer.

Time series are shown (Fig. 2d, e) of MERRA-2 ozone partial column anomalies with the MLR term  $\alpha_0(t)$  removed, summed for the layer between 0.5 and 9.5 km above the tropopause and averaged in the two latitude bands 50°S–20°S and 20°N–60°N (arithmetic average with no weighting). Also shown are the corresponding ozone time series reconstructed from the MLR, demonstrating that the regression model realistically captures the interannual variability. Despite the large variability, there are significant trends of  $-1.17 \pm 0.33$  DU decade<sup>-1</sup> ( $-1.5 \pm 0.4\%$ ) in the SH and  $-1.67 \pm 0.54$  DU decade<sup>-1</sup> ( $-1.8 \pm 0.6\%$ ) in the NH. The two-sigma trend uncertainties are derived from the MLR using ozone averaged within each region and corrected for autocorrelation. They do not reflect uncertainties in the reanalysis itself or in the proxies. The GEOS-RPIT (M2-GMI) trends calculated for the same SH and NH regions are  $-1.2 \pm 0.35$  ( $-1.62 \pm 0.48$ ) DU decade<sup>-1</sup>, and  $-2.33 \pm 0.47$  ( $-2.81 \pm 0.67$ ) DU decade<sup>-1</sup>, respectively. The MERRA-2 values are consistent with those of Ball et al. (2018) (expressed there as ozone change between 1998 and 2016, see their Fig. 2) and the GEOS-RPIT and M2-GMI trends are stronger, closer to the far negative tail of the distribution found by Ball et al. (2018). There is a partial cancellation between the LS and the positive trends above in MERRA-2, resulting in a stratospheric total-ozone trend pattern that is positive ( $2.56 \pm 0.52$  DU decade<sup>-1</sup>) between 60°S and the Equator and slightly negative ( $-0.48 \pm 0.48$  DU decade<sup>-1</sup>, at the threshold of statistical significance) between the Equator and 60°N. The corresponding results for GEOS-RPIT (M2-GMI) are  $1.79 \pm 0.51$  DU ( $1.72 \pm 0.54$  DU) south of the equator and  $-1.38 \pm 0.9$  DU ( $-0.49 \pm 0.5$  DU) north of the equator. All three GEOS products show an overall positive ozone trend in the stratosphere. These trends are computed as cosine-weighted averages over the appropriate latitude bands. Note that the linearity of these trends arises from assumptions in the MLR model and does not imply that the real-world mechanisms involved evolve linearly.

Trend patterns from MERRA-2 exhibit some seasonal variability with the strongest negative trends in the extratropics occurring during winter (Fig. S2), implying that the mechanism responsible has some weak seasonal dependence.

#### 4. Results: Tracer Transport

This section presents an analysis of zonal-mean trends in ozone and e90, expressed as the change of their mixing ratios per decade. The mean gradients, in both the vertical distance above the tropopause and in latitude in each hemisphere, have opposite signs for ozone and e90. Consequently, transport-related trends in ozone and e90 are expected to have opposite signs in the LS.

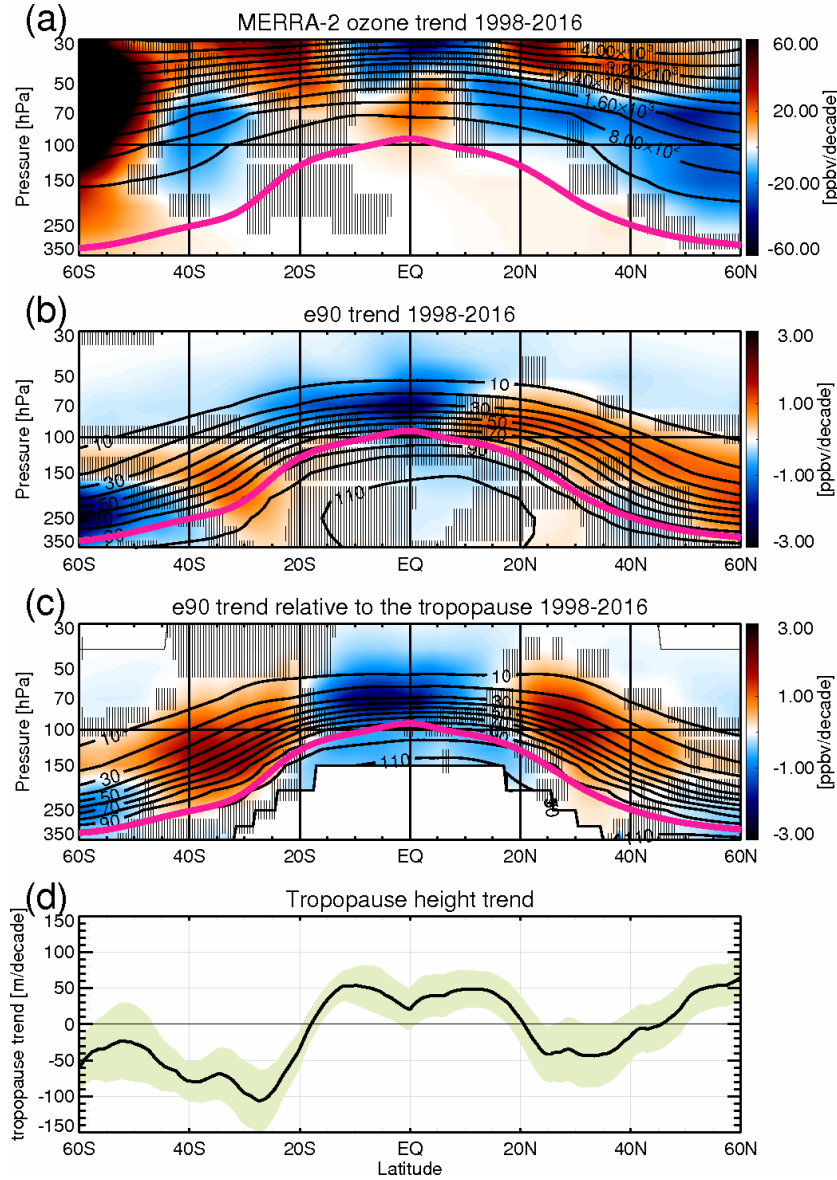


**Figure 3.** (a) 1998-2016 trend in zonally averaged MERRA-2 ozone mixing ratio (ppbv decade<sup>-1</sup>) (colors) and the mean ozone (contours; ppbv) as a function of latitude and pressure. (b) Trend in zonally averaged M2-GMI e90 (colors) and zonal mean e90 mixing ratio (contours) as a function of latitude and pressure. (c) e90 trend and mixing ratio calculated in the tropopause-relative vertical coordinate and remapped to pressure levels using the climatological MERRA-2 tropopause. The tropopause is shown in magenta. Stippling in (a-c) indicates the regions where the trends are not significant at 95%. (d) MERRA-2 tropopause height trend as a function of latitude. The 2-sigma envelope is shown in light green.

Figure 3 shows the trends calculated for MERRA-2 ozone mixing ratio, e90 and the tropopause height. The ozone trend (Fig. 3a) is positive between 10°S and 10°N and negative in the extratropics between 45°S and 30°S and between 15°N and 60°N, and these results are significant over most of the NH and in a more confined region of the SH. The strongest negative trend of -27 parts per billion per decade (ppbv decade<sup>-1</sup>) (-2.1%) is seen at 70 hPa between 20°N and 60°N. The trend pattern for e90 (Fig. 3b) is very similar to that for ozone, but with opposite sign: negative trends in ozone correspond to positive trends in e90 and vice versa. The NH trends are stronger and extend further poleward than the SH ones for both ozone and e90. Finally, the 350–150 hPa layer between 60°S and 40°S shows a positive ozone trend and negative e90 trend. Since changes in e90 are controlled solely by transport, those similarities strongly suggest that the LS ozone trends in MERRA-2 are also driven primarily by decadal-scale changes in the LS circulation.

Abalos et al. (2017) showed that long-term changes in the zonal-mean LS tracer concentrations are highly sensitive to tropopause displacements. For example, for tracers with negative vertical gradients like e90, an upward shift in the tropopause will result in a positive tracer anomaly at a given pressure level, independent of other circulation changes. In order to separate the effects of the tropopause movements from those induced by circulation changes, the e90 trends were calculated in the TR vertical coordinate and remapped to pressure levels using the climatological MERRA-2 tropopause (Fig. 3c). If the trend in e90 (or any other tracer) were entirely due to a tropopause shift, it would vanish when computed in TR coordinates. Trends in the tropopause height (Fig. 3d), along with their 2-sigma envelope, in conjunction with the e90 trends (Fig. 3b and 3c) show that the upward shift of the tropopause between 50°N and 60°N enhances the positive e90 trends in the pressure coordinate (compared to the TR coordinate) in the LS in this latitude band. Similarly, the upward displacement in the Tropics slightly reduces the negative e90 trend. Conversely, the downward shift in the SH extratropics reduces the positive trend there. The Tropics-extratropics contrast is enhanced and more symmetric with respect to the Equator in the TR coordinates. It follows that the ozone and e90 trends (Fig. 3c) are attributable mainly to changes in the large-scale circulation rather than tropopause displacements.

This trend pattern, with tropical reductions and extratropical increases in e90 concentrations, is consistent with enhanced tropical-to-extratropical isentropic transport over the period 1998-2016. A similar conclusion can be drawn from the changes in another passive tracer (st80\_25), that is set to a constant value at pressures lower than 80 hPa and subject to a uniform exponential decay rate of 25 days<sup>-1</sup> below the tropopause, as described in Eyring et al. (2013). Consistent with enhanced quasi-horizontal isentropic transport, the trends in st80\_25 are negative throughout the extratropical lower stratosphere (north of 50°S in SH), reflecting enhanced dilution of high st80\_25 extratropical air masses with low (tropical) values of st80\_25 (Fig. S3). This mechanism is discussed further in Section 5.

## 5. Discussion and Conclusions

There is a discernible trend in lower stratospheric ozone profiles in MERRA-2 over the period 1998-2016 when ODSs are no longer increasing. MERRA-2 ozone exhibits a statistically significant negative trend of  $-1.17 \text{ DU decade}^{-1}$  in a 10-km deep layer above the tropopause between  $50^{\circ}\text{S}$  and  $20^{\circ}\text{S}$  and a stronger trend of  $-1.67 \text{ DU decade}^{-1}$  between  $20^{\circ}\text{N}$  and  $60^{\circ}\text{N}$  in agreement with the findings in Ball et al. (2018). Similar (albeit up to 1.5 times stronger) trends are also detected in a MERRA-2-related ozone dataset – the GEOS-RPIT and in a MERRA-2 driven chemistry model simulation, M2-GMI. In the Tropics, the trend pattern consists of a dipole of increased ozone in the LS and decreased ozone in a shallower 5-km layer above the tropopause. While these long-term changes are modulated by decadal-scale changes in tropopause height, the ozone and passive tracer trends are evident in both tropopause relative and pressure coordinate systems.

As shown by Birner and Bönisch (2011), large-scale transport between the Tropics and the extratropics in the LS is controlled by the shallow branch of the Brewer-Dobson circulation, which consists of mean advection by the residual circulation (RC) and two-way mixing by eddies (Plumb et al., 2002; Butchart, 2014), both driven by synoptic-scale wave breaking. The ozone (and e90) trend pattern seen in Fig. 3 is consistent with either a slowdown of the RC or an intensification of two-way mixing between the tropical and extratropical LS. A preliminary analysis of the RC in MERRA-2 (not shown) suggests there is an increase in downwelling in the extratropics and a slightly weakened upwelling in the Tropical LS. This explains the positive ozone trend in the Tropics but not the negative trend in the extratropics, which is, rather, more likely a reflection of enhanced two-way transport. Such an intensification of the shallow branch of the Brewer-Dobson Circulation in recent decades has been reported by Bönisch et al. (2011), Diallo et al. (2012), Ray et al. (2014) and Ploeger et al. (2015); it is consistent with projected circulation increases in response to future increases in greenhouse gases (Butchart et al., 2010) but may also be a transient phenomenon. The proposed mechanism is in accord with previous studies that have shown that effective diffusivity, a measure of the two-way mixing, increases in the LS over the recent decades (Ray et al. 2010, their Figure 7). In particular, Ray et al. (2014) and Ploeger et al. (2015) find that changes in isentropic mixing have contributed to recent observed mean age trends in the LS. Most recently, Stiller et al. (2017) suggest that these changes are connected to a southward shift of the Brewer-Dobson circulation. As such a shift may also imply changes in lower-stratospheric mixing, however, this finding is not necessarily inconsistent with the ones discussed in the earlier studies.

The primary role of transport does not preclude a potential role of other factors, such as chemistry. However, at least in M2-GMI, the chemical ozone tendencies do not exhibit a statistically significant trend toward stronger depletion in the LS.

While there are some overall similarities with the results of Ball et al. (2018), important quantitative differences exist. First, the negative trends found in the GEOS products in the extratropics are mainly confined to the layer between the tropopause and 50 hPa; in Ball et al (2018) they extend to about 30 hPa. Second, the approximately 5-km layer of positive trend in the Tropics seen in Figs. 2 and 3, which is absent in Ball et al. (2018), is consistent with both the behavior of e90 (Fig. 3) and ozonesonde data (Fig. 1). It is conceivable that this structure is captured by the relatively high vertical resolution of the GEOS products compared to that of the

merged satellite data sets. Third, unlike Ball et al. (2018), the MERRA-2 analysis does not show evidence of an overall decline of stratospheric ozone: the trend is positive in the SH extratropics and only slightly negative ( $-0.66$  DU decade<sup>-1</sup>) in the NH. Finally, Ball et al. (2018) noted that the negative ozone trends in the LS were not present in The Whole Atmosphere Community Climate Model simulations with specified dynamics from MERRA and MERRA-2, but the M2-GMI results do show this trend. These differences require further investigation.

We note that changes in the MERRA-2 observing system, particularly in the assimilated radiance data that occur over the period of the reanalysis may have an impact on the long-term behavior of stratospheric transport patterns. This underscores the need for independent verification of changes in mixing, such as from in-situ observations of trace gases.

To date, no other published work has used reanalysis ozone to study vertically resolved trends in the stratosphere. This study is intended as the first step towards comprehensive application of atmospheric reanalyses to investigations of long-term changes in ozone profiles in the context of stratospheric dynamics and chemistry in the changing climate.

## Acknowledgements

MERRA-2 is an official product of the Global Modeling and Assimilation Office at NASA GSFC, supported by NASA's Modeling, Analysis and Prediction (MAP) program in addition to supporting M2-GMI. Resources supporting this work were provided by the NASA High-End Computing (HEC) Program through the NASA Center for Climate Simulation (NCCS) at Goddard Space Flight Center. The reanalysis data are available at <https://disc.sci.gsfc.nasa.gov/>. M2-GMI and GEOS-RIPT data are available upon request. We are grateful to the National Oceanic and Atmospheric Administration for providing homogenized ozonesonde data. The ozonesonde data were downloaded from <ftp://aftp.cmdl.noaa.gov/data/ozwv/Ozonesonde/>. The aerosol optical depth data were obtained from <https://eosweb.larc.nasa.gov/>. The  $RF_{10.7}$  data are from the Natural Resources Canada (<http://www.spaceweather.ca/solarflux/sx-5-en.php>) obtained through the Royal Netherlands Meteorological Institute Climate Explorer database (<http://climexp.knmi.nl>) and the MEI time series were downloaded from the National Oceanic and Atmospheric Administration's website <https://www.esrl.noaa.gov/psd/enso/mei/>. We thank Brad Weir and Christoph Keller of GMAO for helpful discussions and two anonymous reviewers for their extremely insightful comments and suggestions.

## References

- Abalos, M., W.J. Randel, D.E. Kinnison, and R.R. Garcia (2017), Using the Artificial Tracer e90 to Examine Present and Future UTLS Tracer Transport in WACCM. *J. Atmos. Sci.*, **74**, 3383–3403, doi:10.1175/JAS-D-17-0135.1.
- Bai, K., N.-B. Chang, R. Shi, H. Yu, and W. Gao (2017), An intercomparison of multidecadal observational and reanalysis data sets for global total ozone trends and variability analysis, *J. Geophys. Res. Atmos.*, **122**, 7119–7139, doi:10.1002/2016JD025835.

460 Ball, W. T., Alsing, J., Mortlock, D. J., Rozanov, E. V., Tummon, F., and Haigh, J. D. (2017),  
 461 Reconciling differences in stratospheric ozone composites. *Atmos. Chem. Phys.*, *17*, 12269-  
 462 12302, doi:10.5194/acp-17-12269-2017.

463 Ball, W. T., Alsing, J., Mortlock, D. J., Staehelin, J., Haigh, J. D., Peter, T., Tummon, F., Stübi,  
 464 R., Stenke, A., Anderson, J., Bourassa, A., Davis, S. M., Degenstein, D., Frith, S.,  
 465 Froidevaux, L., Roth, C., Sofieva, V., Wang, R., Wild, J., Yu, P., Ziemke, J. R., and Rozanov,  
 466 E. V. (2018), Evidence for a continuous decline in lower stratospheric ozone offsetting ozone  
 467 layer recovery, *Atmos. Chem. Phys.*, *18*, 1379-1394, [https://doi.org/10.5194/acp-18-1379-](https://doi.org/10.5194/acp-18-1379-2018)  
 468 2018

469  
 470 Birner, T. and Bönisch, H. (2011), Residual circulation trajectories and transit times into the  
 471 extratropical lowermost stratosphere, *Atmos. Chem. Phys.*, *11*, 817-827, doi:10.5194/acp-11-  
 472 817-2011.

473  
 474 Bloom, S., L. Takacs, A. DaSilva, and D. Ledvina (1996), Data as- simulation using incremental  
 475 analysis updates. *Mon. Wea. Rev.*, *124*, 1256–1271, doi:10.1175/1520-0493(1996)124,1256:  
 476 DAUIAU.2.0.CO;2.

477 Bosilovich, M., Akella, S., Coy, L., Cullather, R., Draper, C., Gelaro, R., Kovach, R., Liu, Q.,  
 478 Molod, A., Norris, P., Wargan, K., Chao, W., Reichle, R., Takacs, L., Vikhliayev, Y., Bloom,  
 479 S., Collow, A., Firth, S., Labow, G., Partyka, G., Pawson, S., Reale, O., Schubert, S. D., and  
 480 Suarez, M. (2015), MERRA-2: Initial Evaluation of the Climate, Series on Global Modeling  
 481 and Data Assimilation, *NASA/TM–2015-104606, Vol. 43*, NASA.

482 Bönisch, H., Engel, A., Birner, Th., Hoor, P., Tarasick, D. W., and Ray, E. A. (2011), On the  
 483 structural changes in the Brewer-Dobson circulation after 2000, *Atmos. Chem. Phys.*, *11*,  
 484 3937-3948, doi:10.5194/acp-11-3937-2011.

485  
 486 Bourassa, A. E., Degenstein, D. A., Randel, W. J., Zawodny, J. M., Kyrölä, E., McLinden, C. A.,  
 487 Sioris, C. E., and Roth, C. Z. (2014), Trends in stratospheric ozone derived from merged  
 488 SAGE II and Odin-OSIRIS satellite observations, *Atmos. Chem. Phys.*, *14*, 6983-6994,  
 489 doi:10.5194/acp-14-6983-2014.

490  
 491 Bourassa, A. E., Roth, C. Z., Zawada, D. J., Rieger, L. A., McLinden, C. A., and Degenstein, D.  
 492 A. (2018), Drift-corrected Odin-OSIRIS ozone product: algorithm and updated stratospheric  
 493 ozone trends, *Atmos. Meas. Tech.*, *11*, 489-498, <https://doi.org/10.5194/amt-11-489-2018>.

494  
 495 Butchart, N., et al. (2010), Chemistry-climate model simulations of twenty-first century  
 496 stratospheric climate and circulation changes, *J. Clim.*, *23*, 5349–5374,  
 497 doi:10.1175/2010JCLI3404.1.

498  
 499 Butchart, N. (2014), The Brewer-Dobson circulation, *Rev. Geophys.*, *52*,  
 500 doi:10.1002/2013RG000448.

501  
 502 Davis, S. M., Hegglin, M. I., Fujiwara, M., Dragani, R., Harada, Y., Kobayashi, C., Long, C.,

503 Manney, G. L., Nash, E. R., Potter, G. L., Tegtmeier, S., Wang, T., Wargan, K., and Wright,  
 504 J. S. (2017), Assessment of upper tropospheric and stratospheric water vapor and ozone in  
 505 reanalyses as part of S-RIP, *Atmos. Chem. Phys.*, *17*, 12743-12778, doi:10.5194/acp-17-  
 506 12743-2017.

507 de Laat, A. T. J., van Weele, M., & van der A, R. J. (2017), Onset of stratospheric ozone recovery  
 508 in the Antarctic ozone hole in assimilated daily total ozone columns. *J. Geophys. Res.*, *122*.  
 509 doi:10.1002/2016JD025723

510 Diallo, M., Legras, B., and Chédin, A. (2012), Age of stratospheric air in the ERA-Interim,  
 511 *Atmos. Chem. Phys.*, *12*, 12133-12154, doi:10.5194/acp-12-12133-2012.

512 Douglass, A. R., R. S. Stolarski, S. E. Strahan, and P. S. Connell (2004), Radicals and reservoirs  
 513 in the GMI chemistry and transport model: Comparison to measurements, *J. Geo-phys. Res.*,  
 514 *109*, D16302, doi:10.1029/2004JD004632.

515 Gelaro, R., W. McCarty, M.J. Suárez, R. Todling, A. Molod, L. Takacs, C.A. Randles, A.  
 516 Darmenov, M.G. Bosilovich, R. Reichle, K. Wargan, L. Coy, R. Cullather, C. Draper, S.  
 517 Akella, V. Buchard, A. Conaty, A.M. da Silva, W. Gu, G. Kim, R. Koster, R. Lucchesi, D.  
 518 Merkova, J.E. Nielsen, G. Partyka, S. Pawson, W. Putman, M. Rienecker, S.D. Schubert, M.  
 519 Sienkiewicz, and B. Zhao (2017), The Modern-Era Retrospective Analysis for Research and  
 520 Applications, Version 2 (MERRA-2). *J. Climate*, *30*, 5419–5454, doi:10.1175/JCLI-D-16-  
 521 0758.1

522 Hegglin, M. I., Plummer, D. A., Shepherd, T. G., Scinocca, J. F., Anderson, J., Froidevaux, L.,  
 523 Funke, B., Hurst, D., Rozanov, A., Urban, J., von Clarmann, T., Walker, K. A., Wang, H. J.,  
 524 Tegtmeier, S., and Weigel, K. (2014), Vertical structure of stratospheric water vapour trends  
 525 derived from merged satellite data, *Nature Geoscience*, *7*, 768–776, doi:10.1038/ngeo2236.  
 526

527 Hubert, D., Lambert, J.-C., Verhoelst, T., Granville, J., Keppens, A., Baray, J.-L., Bourassa, A.  
 528 E., Cortesi, U., Degenstein, D. A., Froidevaux, L., Godin-Beekmann, S., Hoppel, K. W.,  
 529 Johnson, B. J., Kyrölä, E., Leblanc, T., Lichtenberg, G., Marchand, M., McElroy, C. T.,  
 530 Murtagh, D., Nakane, H., Portafaix, T., Querel, R., Russell III, J. M., Salvador, J., Smit, H.  
 531 G. J., Stebel, K., Steinbrecht, W., Strawbridge, K. B., Stübi, R., Swart, D. P. J., Taha, G.,  
 532 Tarasick, D. W., Thompson, A. M., Urban, J., van Gijssel, J. A. E., Van Malderen, R., von der  
 533 Gathen, P., Walker, K. A., Wolfram, E., and Zawodny, J. M. (2016), Ground-based  
 534 assessment of the bias and long-term stability of 14 limb and occultation ozone profile data  
 535 records, *Atmos. Meas. Tech.*, *9*, 2497-2534, <https://doi.org/10.5194/amt-9-2497-2016>.  
 536

537 Eyring, V., Cionni, I., Bodeker, G. E., Charlton-Perez, A. J., Kinnison, D. E., Scinocca, J. F.,  
 538 Waugh, D. W., Akiyoshi, H., Bekki, S., Chipperfield, M. P., Dameris, M., Dhomse, S., Frith,  
 539 S. M., Garny, H., Gettelman, A., Kubin, A., Langematz, U., Mancini, E., Marchand, M.,  
 540 Nakamura, T., Oman, L. D., Pawson, S., Pitari, G., Plummer, D. A., Rozanov, E., Shepherd,  
 541 T. G., Shibata, K., Tian, W., Braesicke, P., Hardiman, S. C., Lamarque, J. F., Morgenstern,  
 542 O., Pyle, J. A., Smale, D., and Yamashita, Y. (2010), Multi-model assessment of stratospheric

543 ozone return dates and ozone recovery in CCMVal-2 models, *Atmos. Chem. Phys.*, *10*, 9451-  
544 9472, doi:10.5194/acp-10-9451-2010.

545

546 Eyring, V., and Coauthors (2013), Overview of IGAC/SPARC Chemistry-Climate Model  
547 Initiative (CCMI) community simulations in support of upcoming ozone and climate  
548 assessments. *SPARC newsletter*, *40* (January), 48–66.

549

550 Fröhlich, C. (2000), Observations of Irradiance Variations, *Space Science Reviews* *94*: 15,  
551 doi:10.1023/A:1026765712084.

552

553 Froidevaux, L., and Coauthors (2008), Validation of Aura Micro- wave Limb Sounder  
554 stratospheric ozone measurements. *J. Geophys. Res.*, *113*, D15S20,  
555 doi:10.1029/2007JD008771.

556 Global Modeling and Assimilation Office (GMAO 2015a), MERRA-2 inst3\_3d\_asm\_Nv: 3d,3-  
557 Hourly,Instantaneous,Model-Level,Assimilation,Assimilated Meteorological Fields V5.12.4,  
558 Greenbelt, MD, USA, *Goddard Earth Sciences Data and Information Services Center (GES*  
559 *DISC)*, Accessed: December 2017, doi:10.5067/WWQSQ8IVFW8.

560

561 Global Modeling and Assimilation Office (GMAO 2015b), MERRA-2 instM\_3d\_asm\_Np:  
562 3d,Monthly mean,Instantaneous,Pressure-Level,Assimilation,Assimilated Meteorological  
563 Fields V5.12.4, Greenbelt, MD, USA, *Goddard Earth Sciences Data and Information*  
564 *Services Center (GES DISC)*, Accessed: December 2017, doi:10.5067/2E096JV59PK7.

565

566 Hall, T.M., and R.A. Plumb (1994), Age as a diagnostic of stratospheric transport. *J. Geophys.*  
567 *Res.*, *99*, 1059-1070, doi:10.1029/93JD03192.

568 Harris, N. R. P., Hassler, B., Tummon, F., Bodeker, G. E., Hubert, D., Petropavlovskikh, I.,  
569 Steinbrecht, W., Anderson, J., Bhartia, P. K., Boone, C. D., Bourassa, A., Davis, S. M.,  
570 Degenstein, D., Delcloo, A., Frith, S. M., Froidevaux, L., Godin-Beekmann, S., Jones, N.,  
571 Kurylo, M. J., Kyrölä, E., Laine, M., Leblanc, S. T., Lambert, J.-C., Liley, B., Mahieu, E.,  
572 Maycock, A., de Mazière, M., Parrish, A., Querel, R., Rosenlof, K. H., Roth, C., Sioris, C.,  
573 Staehelin, J., Stolarski, R. S., Stübi, R., Tamminen, J., Vigouroux, C., Walker, K. A., Wang,  
574 H. J., Wild, J., and Zawodny, J. M. (2015), Past changes in the vertical distribution of ozone –  
575 Part 3: Analysis and interpretation of trends, *Atmos. Chem. Phys.*, *15*, 9965-9982,  
576 doi:10.5194/acp-15-9965-2015.

577

578 Kleist, D. T., D. F. Parrish, J. C. Derber, R. Treadon, W.-S. Wu, and S. Lord (2009), In-  
579 troduction of the GSI into the NCEPs Global Data Assimilation System. *Wea. Forecasting*,  
580 *24*, 1691–1705, doi:10.1175/2009WAF2222201.1.

581 Levelt, P. F., and Coauthors (2006), The ozone monitoring in- strument. *IEEE Trans. Geosci.*  
582 *Remote Sens.*, *44*, 1093–1101, doi:10.1109/TGRS.2006.872333.

583 Long, C. S., Fujiwara, M., Davis, S., Mitchell, D. M., and Wright, C. J. (2017), Climatology and  
584 interannual variability of dynamic variables in multiple reanalyses evaluated by the SPARC  
585 Reanalysis Intercomparison Project (S-RIP), *Atmos. Chem. Phys.*, *17*, 14593-14629,



doi:10.5194/acp-17-14593-2017.

McCarty, W., L. Coy, R. Gelaro, A. Huang, D. Merkova, E. B. Smith, M. Sienkiewicz, and K. Wargan (2016), MERRA-2 input observations: Summary and initial assessment. *Technical Report Series on Global Modeling and Data Assimilation, Vol. 46, NASA Tech. Rep. NASA/TM-2016-104606, 61 pp.* [Available online at <https://gmao.gsfc.nasa.gov/pubs/docs/McCarty885.pdf>.]

Molod, A., Takacs, L., Suarez, M., and Bacmeister, J. (2015), Development of the GEOS- 5 atmospheric general circulation model: evolution from MERRA to MERRA2, *Geosci. Model Dev.*, 8, 1339–1356, doi:10.5194/gmd-8-1339-2015.

Naujokat, B. (1986), An Update of the Observed Quasi-Biennial Oscillation of the Stratospheric Winds over the Tropics. *J. Atmos. Sci.*, **43**, 1873–1877, doi:10.1175/1520-0469(1986)043<1873:AUOTOQ>2.0.CO;2

Nielsen, J. E., Pawson, S., Molod, A., Auer, B., da Silva, A. M., Douglass, A. R., ... Wargan, K. (2017), Chemical mechanisms and their applications in the Goddard Earth Observing System (GEOS) earth system model. *Journal of Advances in Modeling Earth Systems*, 9, doi:10.1002/2017MS001011.

Oman, L. D. and coauthors (2010), Multimodel assessment of the factors driving stratospheric ozone evolution over the 21st century, *J. Geophys. Res.*, **115**, D24306, doi:10.1029/2010JD014362.

Orbe, C., Oman, L. D., Strahan, S. E., Waugh, D. W., Pawson, S., Takacs, L. L., & Molod, A. M. (2017), Large-scale atmospheric transport in GEOS replay simulations. *Journal of Advances in Modeling Earth Systems*, 9, doi:10.1002/2017MS001053

Ploeger, F., M. Riese, F. Haenel, P. Konopka, R. Müller, and G. Stiller (2015), Variability of stratospheric mean age of air and of the local effects of residual circulation and eddy mixing, *J. Geophys. Res. Atmos.*, **120**, 716–733, doi:10.1002/2014JD022468.

Plumb, R. A. (2002), Stratospheric transport, *J. Meteorol. Soc. Jpn.*, **80**(4B), 793–809.

Prather, M. J., X. Zhu, Q. Tang, J. Hsu, and J. L. Neu (2011), An atmospheric chemist in search of the tropopause. *J. Geophys. Res.*, **116**, D04306, doi:10.1029/2010JD014939.

Randel, W. J., and A. M. Thompson (2011), Interannual variability and trends in tropical ozone derived from SAGE II satellite data and SHADOZ ozonesondes, *J. Geophys. Res.*, **116**, D07303, doi:10.1029/2010JD015195.

Ray, E. A., et al. (2010), Evidence for changes in stratospheric transport and mixing over the past three decades based on multiple data sets and tropical leaky pipe analysis, *J. Geophys. Res.*, **115**, D21304, doi:10.1029/2010JD014206.

Ray, E. A., et al. (2014), Improving stratospheric transport trend analysis based on SF<sub>6</sub> and CO<sub>2</sub> measurements, *J. Geophys. Res. Atmos.*, **119**, 14,110–14,128, doi:10.1002/2014JD021802.

625 Sofieva, V. F., Kyrölä, E., Laine, M., Tamminen, J., Degenstein, D., Bourassa, A., Roth, C.,  
 626 Zawada, D., Weber, M., Rozanov, A., Rahpoe, N., Stiller, G., Laeng, A., von Clarmann, T.,  
 627 Walker, K. A., Sheese, P., Hubert, D., van Roozendaal, M., Zehner, C., Damadeo, R.,  
 628 Zawodny, J., Kramarova, N., and Bhartia, P. K. (2017), Merged SAGE II, Ozone\_cci and  
 629 OMPS ozone profile dataset and evaluation of ozone trends in the stratosphere, *Atmos. Chem.*  
 630 *Phys.*, *17*, 12533-12552, doi:10.5194/acp-17-12533-2017.  
 631  
 632 Steinbrecht, W., Froidevaux, L., Fuller, R., Wang, R., Anderson, J., Roth, C., Bourassa, A.,  
 633 Degenstein, D., Damadeo, R., Zawodny, J., Frith, S., McPeters, R., Bhartia, P., Wild, J.,  
 634 Long, C., Davis, S., Rosenlof, K., Sofieva, V., Walker, K., Rahpoe, N., Rozanov, A., Weber,  
 635 M., Laeng, A., von Clarmann, T., Stiller, G., Kramarova, N., Godin-Beekmann, S., Leblanc,  
 636 T., Querel, R., Swart, D., Boyd, I., Hocke, K., Kämpfer, N., Maillard Barras, E., Moreira, L.,  
 637 Nedoluha, G., Vigouroux, C., Blumenstock, T., Schneider, M., García, O., Jones, N., Mahieu,  
 638 E., Smale, D., Kotkamp, M., Robinson, J., Petropavlovskikh, I., Harris, N., Hassler, B.,  
 639 Hubert, D., and Tummon, F. (2017), An update on ozone profile trends for the period 2000 to  
 640 2016, *Atmos. Chem. Phys.*, *17*, 10675-10690, doi:10.5194/acp-17-10675-2017.  
 641  
 642 Sterling, C. W., Johnson, B. J., Oltmans, S. J., Smit, H. G. J., Jordan, A. F., Cullis, P. D., Hall, E.  
 643 G., Thompson, A. M., and Witte, J. C. (2017), Homogenizing and Estimating the Uncertainty  
 644 in NOAA's Long Term Vertical Ozone Profile Records Measured with the Electrochemical  
 645 Concentration Cell Ozone sonde, *Atmos. Meas. Tech. Discuss.*, doi:10.5194/amt-2017-397, in  
 646 review.  
 647  
 648 Stiller, G. P., Fierli, F., Ploeger, F., Cagnazzo, C., Funke, B., Haenel, F. J., Reddmann, T., Riese,  
 649 M., and von Clarmann, T. (2017), Shift of subtropical transport barriers explains observed  
 650 hemispheric asymmetry of decadal trends of age of air, *Atmos. Chem. Phys.*, *17*, 11177-  
 11192, <https://doi.org/10.5194/acp-17-11177-2017>  
 651  
 652 Stolarski, R. S., P. Bloomfield, R. D. McPeters and J. R. Herman (1991), Total ozone trends  
 653 deduced from Nimbus 7 TOMS data, *Geophys. Res. Lett.*, *18*, 1015-1018,  
 doi:10.1029/91GL01302.  
 654  
 655 Thomason, L. W., Ernest, N., Millán, L., Rieger, L., Bourassa, A., Vernier, J.-P., Manney, G.,  
 656 Luo, B., Arfeuille, F., and Peter, T. (2018), A global, space-based stratospheric aerosol  
 657 climatology: 1979 to 2016, *Earth Syst. Sci. Data Discuss.*, <https://doi.org/10.5194/essd-2017-91>.  
 658  
 659 Thompson, A. M., Witte, J. C., Sterling, C., Jordan, A., Johnson, B. J., Oltmans, S. J., ... Thiongo,  
 660 K. (2017). First reprocessing of Southern Hemisphere Additional Ozone sondes (SHADOZ)  
 661 ozone profiles (1998–2016): 2. Comparisons with satellites and ground-based instruments.  
 662 *Journal of Geophysical Research: Atmospheres*, *122*, 13,000–13,025. <https://doi.org/10.1002/2017JD027406>  
 663  
 664 Wallace, J. M., R. L. Panetta, and J. Estberg (1993) Representation of the equatorial stratospheric  
 665 quasi-biennial oscillation in EOF phase space, *J. Atmos. Sci.*, *50*, 1751--1762,  
 doi:10.1175/1520-0469(1993)050<1751:ROTESQ>2.0.CO.

- Wargan, K., G. Labow, S. Frith, S. Pawson, N. Livesey, and G. Partyka (2017), Evaluation of the Ozone Fields in NASA's MERRA-2 Reanalysis. *J. Climate*, *30*, 2961–2988, doi:10.1175/JCLI-D-16-0699.1
- Waters, J. W., and Coauthors (2006), The Earth Observing System Microwave Limb Sounder (EOS MLS) on the Aura satellite. *IEEE Trans. Geosci. Remote Sens.*, *44*, 1075–1092, doi:10.1109/TGRS.2006.873771.
- Weatherhead, E. C., *et al.* (1998), Factors affecting the detection of trends: Statistical considerations and applications to environmental data, *J. Geophys. Res.*, *103*(D14), 17149–17161, doi:10.1029/98JD00995.
- Witte, J. C., *et al.* (2017), First reprocessing of Southern Hemisphere Additional Ozone sondes (SHADOZ) profile records (1998–2015): 1. Methodology and evaluation, *J. Geophys. Res. Atmos.*, *122*, 6611–6636, doi:10.1002/2016JD026403.
- Wolter, K., and M. S. Timlin (1998), Measuring the strength of ENSO events - how does 1997/98 rank? *Weather*, **53**, 315–324
- World Meteorological Organization (WMO 2014): Scientific Assessment of Ozone Depletion: 2014. *Global Ozone Research and Monitoring Project – Report no. 55*
- Wu, W., R.J. Purser, and D.F. Parrish (2002), Three-Dimensional Variational Analysis with Spatially Inhomogeneous Covariances. *Mon. Wea. Rev.*, *130*, 2905–2916, doi:10.1175/1520-0493(2002)130<2905:TDVAWS>2.0.CO;2.

## Figure captions

**Figure 1.** Time series of annual ozone anomalies at Trinidad Head (**a, d, g**), Boulder (**b, e, h**) and Pago Pago (**c, f**) at 70 hPa (**a, b, c**), 100 hPa (**d, e, f**) and 200 hPa (**g, h**) from ozonesondes (black), bias-corrected MERRA-2 (blue), M2-GMI (red) and bias-corrected GEOS-RPIT (yellow). The anomalies for each data set are calculated by subtracting the average of that data set. The corresponding least-squares fit lines are dashed and the  $R^2$  values are shown in each panel.

**Figure 2. (a-c):** Zonally and annually averaged ozone trends as a function of latitude and height above the tropopause derived from **(a)** MERRA-2, **(b)** GEOS-RPIT and **(c)** M2-GMI using multiple linear regression (colors). Averaged ozone in DU km<sup>-1</sup> is shown as contours. Locations where the trend is not significant at the 2-sigma level are marked by 'X'. **(d-e):** Time series of deseasonalized partial column ozone from MERRA-2 between 0.5 km and 9.5 km above the tropopause (black) averaged between **(d)** 50°S – 20°S and **(e)** 20°N – 60°N (within the white boxes in panel a). The magenta curves show ozone reconstructed from the MLR coefficients and the trends averaged over the same latitude bands are shown in red.

**Figure 3. (a)** 1998-2016 trend in zonally averaged MERRA-2 ozone mixing ratio (ppbv decade<sup>-1</sup>) (colors) and the mean ozone (contours; ppbv) as a function of latitude and pressure. **(b)** Trend in zonally averaged M2-GMI e90 (colors) and zonal mean e90 mixing ratio (contours) as a function of latitude and pressure. **(c)** e90 trend and mixing ratio calculated in the tropopause-relative vertical coordinate and remapped to pressure levels using the climatological MERRA-2 tropopause. The tropopause is shown in magenta. Stippling in **(a-c)** indicates the regions where the trends are not significant at 95%. **(d)** MERRA-2 tropopause height trend as a function of latitude. The 2-sigma envelope is shown in light green.

## **Recent decline in lower stratospheric ozone attributed to circulation changes**

*Krzysztof Wargan<sup>1,2</sup>, Clara Orbe<sup>3</sup>, Steven Pawson<sup>3</sup>, Jerald R. Ziemke<sup>4,5</sup>, Luke D. Oman<sup>6</sup>, Mark A. Olsen<sup>4,5</sup>, Lawrence Coy<sup>1,2</sup>, K. Emma Knowland<sup>6,2</sup>*

<sup>1</sup> Science Systems and Applications Inc., Lanham, Maryland, USA

<sup>2</sup> Global Modeling and Assimilation Office, Code 610.1, NASA Goddard Space Flight Center, Greenbelt, Maryland, USA

<sup>3</sup> Code 611, NASA Goddard Institute for Space Studies, New York, NY, USA

<sup>4</sup> Goddard Earth Science Technology & Research (GESTAR) Morgan State University, Baltimore, MD USA

<sup>5</sup> Atmospheric Chemistry and Dynamics Laboratory, Code 614, NASA Goddard Space Flight Center, Greenbelt, Maryland, USA

<sup>6</sup> Goddard Earth Science Technology & Research (GESTAR), Universities Space Research Association (USRA), Columbia, MD USA

### **Contents of this file**

Details of the bias correction methodology  
Figures S1 to S3

## Details of the bias correction methodology

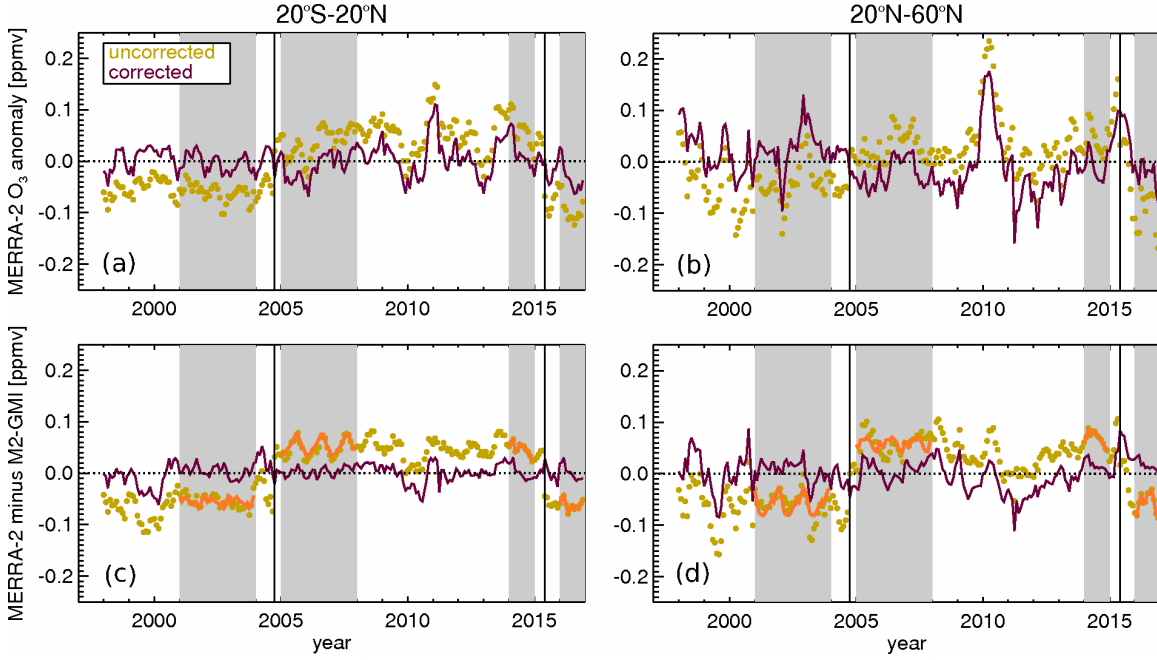


Figure S1. Illustration of the MERRA-2 bias correction using M2-GMI as a transfer function. Plotted are deseasonalized ozone anomaly time series (**a and b**) and their differences with M2-GMI (**c and d**) at 70 hPa averaged between 20°S and 20°N (**a and c**) and between 20°N and 60°N (**b and d**). Uncorrected and bias corrected values are shown as yellow circles and purple lines, respectively. The shaded areas mark the periods of averaging (see text) and the vertical lines indicate the two changes in the ozone observing system. The average differences between the uncorrected MERRA-2 ozone and M2-GMI are shown in orange. The intervals separating the orange lines in the vertical is the bias that the algorithm subtracts from uncorrected MERRA-2.

For each discontinuity, the monthly differences (reanalysis minus M2-GMI) were first calculated at every latitude and level and averaged over three years before ( $\Delta_{\text{before}}$ ) and three years after the discontinuity ( $\Delta_{\text{after}}$ ). The reanalyses were then bias corrected by subtracting the difference  $\Delta = \Delta_{\text{after}} - \Delta_{\text{before}}$  in the period following the discontinuity. This correction was applied to MERRA-2 and GEOS-RIPT at the observing system changes described in Section 2.1. Figure S1 illustrates the procedure and shows the uncorrected (yellow circles) and corrected (purple lines) MERRA-2 ozone at 70 hPa averaged in two latitude bands. The orange lines are the  $\Delta_{\text{before}}$  and  $\Delta_{\text{after}}$  differences. No evidence of remaining discontinuities is seen in the purple lines (panels c and d).

## Additional figures

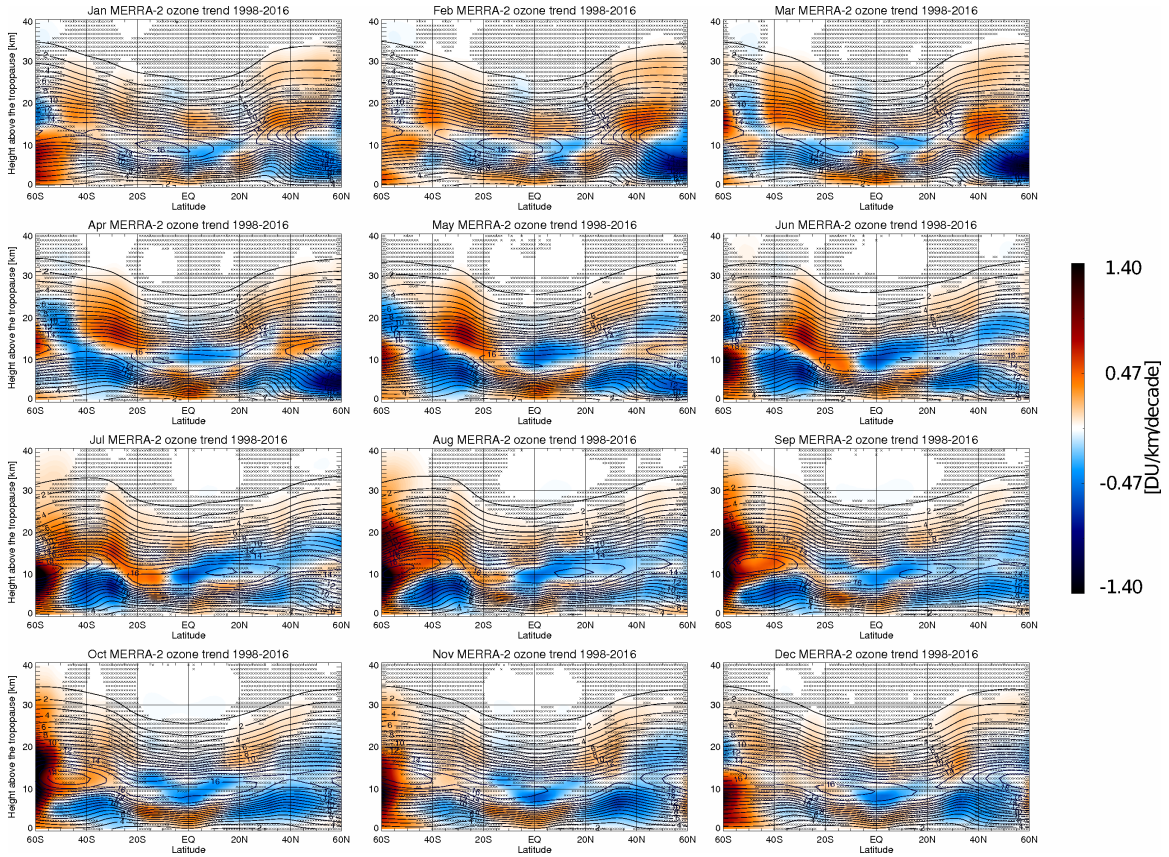
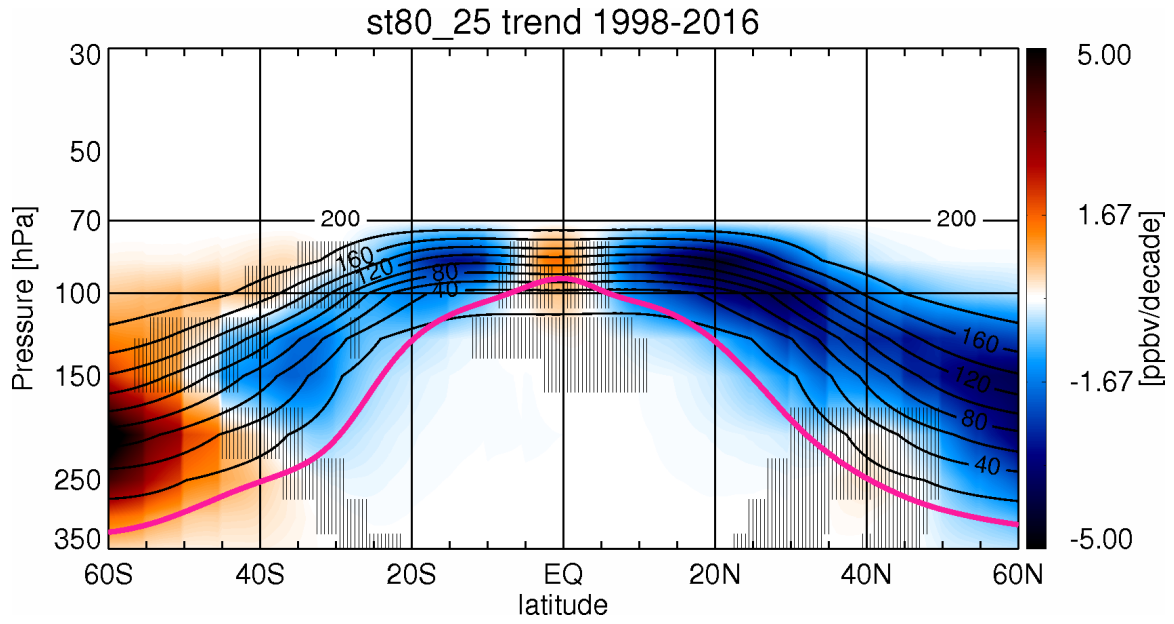


Figure S2. Zonally and annually averaged ozone (contours) and ozone trends (colors) as a function of latitude and height above the tropopause derived from MERRA-2 between 1998 and 2016. The panels show the results for the consecutive calendar months. Ozone is shown in  $\text{DU km}^{-1}$  and the trends in  $\text{DU km}^{-1} \text{ decade}^{-1}$ . Locations where the trend is not significant at the 2-sigma level are marked by 'X'.



**Figure S3.** Trend in zonally averaged M2-GMI tracer *st80\_25* (colors) and zonal mean *st80\_25* mixing ratio (contours) as a function of latitude and pressure. Stippling indicates the regions where the trends are not significant at 95%.